Water Science & Technology

IWA PUBLISHING

Water Science & Technology Vol 84 No 4, 840 doi: 10.2166/wst.2021.274

Modern vision for critical flow in an egg-shaped section

Hachemi Rachedi Lamia [a,*], Lakehal Moussa [b] and Achour Bachir [c]

[a] Laboratory Soil and Hydraulic, Badji Mokhtar University, Annaba B.P.12, Annaba 23000, Algeria
[b] Department of Hydraulic, Research Laboratory in Civil Engineering, Hydraulic, Durable Development and Environment (LARGHYDE), University of Badji Mokhtar Annaba, Annaba, Algeria
[c] Department of Civil and Hydraulic Engineering, Research Laboratory in Subterranean and Surface Hydraulics (LARHYSS), University of Biskra, Biskra, Algeria
*Corresponding author. E-mail: lamia_hrachedi@yahoo.fr

HRL, 0000-0001-8145-9072; LM, 0000-0003-0111-2330; AB, 0000-0002-7290-0468

ABSTRACT

The critical regime plays a primordial role in the study of gradually varying flows by classifying flow regimes and slopes. Through this work, a new approach is proposed to analyze critical flow regime in an egg-shaped channel. Based on both the definition of Froude number and Achour and Bedjaoui general discharge relationship, a relation between critical and normal depths is derived and then graphically represented for the particular case of a smooth channel characterized by a generating diameter equal to 1 m. The results show the influence of the slope on the frequency of occurrence of the critical regime. At the same time and independently of the flow rate, a very advantageous approach for the calculation of the Froude number has been proposed. The study shows that there are six zones to differentiate the various flow states, namely: on the one hand for steep slopes two subcritical zones interspersed by a supercritical zone and on the other hand for mild slopes a zone corresponding to uniform flow, an area where the flow is probably gradually varied and finally an area where the flow is abruptly varied. Based on the specific energy equation, a validation process concluded that the proposed relationships were reliable.

Key words: critical flow, egg-shaped conduit, Froude number, normal flow, rate flow, slope

HIGHLIGHTS

- Determination of the frequency of occurrence of the critical regime.
- The nature of the flow regime can be deduced from the value of the slope.
- New theoretical approach for the study of the critical regime in an egg-shaped conduit considered as a form with several advantages.
- The Froude number can be determined independently of the flow rate. Establishment of an abacus to define the flow domain including non-uniform flows.

1. INTRODUCTION

In nature, water flows in a natural slope whose relief is irregular, creating different types of flows. These flows are classified into two main categories: non-permanent flows whose characteristics vary over time, and permanent flows (French 1985). According to their developments, permanent flows take various aspects: varied or uniform. In practice, uniform flow, with constant geometric and hydraulic characteristics over time and space (Chow 1959; French 1985) is the most studied type. In fact, the study of uniform flow is fundamental in the calculation of various flows (French 1985; Vatankhah 2015). This type of flow is also encountered in pressurized closed channels and at full section. It can also be in subcritical or supercritical regime. Therefore, the critical regime is a particular case of uniform flow where the inertia and gravity forces are in equilibrium. The critical flow plays a significant role in the analysis, design, operation and maintenance of channels (Shang *et al.* 2019). Critical depth computation in open channel is very important to preserve it from erosion caused by unstable critical flow or high kinetic energy (Petikas *et al.* 2020). Several authors have attempted to express the relationship to calculate the critical depth for a given shape of closed or open channel. Based on the expression of Froude number, some authors have attempted to propose a practical method for determining critical depth. Chow (1959) presented a methodology for calculating the critical depth by algebraic method for the rectangular shape and by successive approximations or by graphical method for the more complex forms. Similarly,

Henderson (1966) established a graph for critical depth evaluation in a circular pipe and in a trapezoidal channel for different side slopes. French (1985) reproduced the 1959 Chow diagram and presented the semi-empirical formulas developed by Straub (1982) to calculate critical depth in open channels in rectangular, trapezoidal, triangular, parabolic, circular, elliptical and exponential shape. Heggen (1991) introduced a correction exponent for velocity distribution in the development of the critical depth relationship in rectangular, parabolic and triangular sections. These relationships have been associated with a diagram. However, for the case of trapezoidal channel, the proposed relationship still remains implicit. Swamee (1993) developed explicit critical depth equations for some shapes of irrigation canals. Wang (1998) used an iterative theory to produce an explicit equation for critical depth in a trapezoidal channel. In addition, Swamee & Rathie (2005) proposed exact analytical equations for critical depth calculation in a trapezoidal channel. However, the developed relationships have the disadvantage of being presented in the form of an infinite series. A particularly interesting study was also proposed by Swamee & Swamee (2008) for the explicit calculation of hydraulic parameters for non-circular sewerage pipes including critical depth. Using curve fitting method, Vatankhah & Easa (2011) have proposed explicit solutions for critical and normal depths in trapezoidal, circular, and horseshoe shaped channels. Vatankhah (2015) obtained an explicit solution for computation of critical depth in semi elliptical channels with an excellent approximation of the incomplete wetted perimeter integral. Shang *et al.* (2019) present three explicit solutions for critical depth in closed conduits for circular, arched, and egg-shaped sections. To optimize the model parameters, revised particle swarm optimization (PSO) algorithms have been implemented in MATLAB. Using an adaptive cubic polynomial algorithm (ACPA), Petikas *et al.* (2020) presents a new method for the computation of multiple critical depths in compound and natural channels. Regarding studies discussed previously, only the flow and the geometric parameters are taken into account. However, many other parameters, such as the slope of the channel or conduit, the absolute roughness, and the kinematic viscosity of the flowing liquid can significantly influence the nature of the flow regime. In this regard, these parameters were introduced in the study performed by Nebbar & Achour (2018) concerning the sizing of the rectangular channel under a critical flow regime. Moreover, Achour & Amara (2020) provided new considerations on the critical flow regime in free-surface circular pipe. Indeed, depending on the slope of the pipe, the critical flow regime is not always present in such pipes, as well as for a given diameter and slope, two critical states of the flow can occur for two different flow rates. They also show that there is a slope that generates a single critical state of the flow.

In this context, the present study aims to propose a new approach in the analysis of critical flow and thus to examine the different possibilities of the critical flow state in an egg-shaped conduit. It has been shown in the past that this shape of conduit is suitable for combined sewer sewage networks and present best resistance against traffic loads than usual circular pipes (Regueiro-Picallo *et al.* 2016). In addition, this type of pipe has also improved hydraulic performance in dry weather conditions of normal operation of combined sewer systems, where a high percentage of the discharge time of the flow is carried by the lower part of the section (Butler & Davies 2010). Under these conditions, egg-shaped pipes have higher flow rates due to their smallest wetted perimeter, reducing particle sedimentation and the operational costs of cleaning sewers (Butler & Davies 2010). The resuspension of sewer sediments during wet weather flows is an important source of the pollution of combined sewer overflows (Suarez & Puertas 2005), and their control is one of the main objectives of the integrated urban water management in urban systems (Regueiro-Picallo *et al.* 2016).

2. GEOMETRIC CHARACTERISTICS

The egg shape is complex consisting of three different geometric parts. The flow area, the wetted perimeter and the hydraulic radius are expressed according to the geometrical locus occupied by the flow (Table 1). The flow level may then be in one of the following intervals: zone I: $\eta \leq 1/15$, zone II: $1/15 \leq \eta \leq 2/3$ and zone III: $2/3 \leq \eta \leq 1$. Where $\eta = y/D$ represents the filling rate of the conduit, y the depth of the flow in the conduit and D is the generating diameter. Table 1 represents the different expressions of the geometric characteristics of the conduit, where A is the wetted area, P is the wetted perimeter, T is the top width, and R_h is the hydraulic radius. In addition, the functions $\varphi(\eta)$, $\sigma(\eta)$, $\rho(\eta)$, $\varphi(\eta)$, $\tau(\eta)$, $\lambda(\eta)$, $\vartheta(\eta)$, $\zeta(\eta)$, $\delta(\eta)$ and $\xi(\eta)$ are expressed exclusively as a function of the filling rate η.

3. METHODOLOGY

3.1. Basic equations

The critical regime corresponds to minimum specific energy which is characterized by a Froude number equal to unity. The Froude number is expressed physically as the ratio of the inertial to gravity forces. At critical flow conditions, Froude number

Table 1 | Some common characteristics of the flow in an egg-shaped conduit (Lakehal & Achour 2014). (Note that to distinguish the normal flow from the critical one, the indices '*n*' and '*c*' will be assigned to the relationship)

Zone I : $\eta \leq 1/15$

$T = D\varphi(\eta)$

$\varphi(\eta) = \frac{2}{3}\sqrt{3\eta(1-3\eta)}$

$A = D^2\sigma(\eta)$

$\sigma(\eta) = \frac{1}{36}\left[\cos^{-1}(1-6\eta) - 2(1-6\eta)\sqrt{3\eta(1-3\eta)}\right]$

$P = D\rho(\eta)$

$\rho(\eta) = \frac{1}{3}\cos^{-1}(1-6\eta)$

$R_h = D\frac{\sigma(\eta)}{\rho(\eta)}$

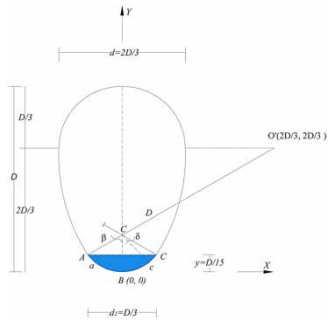

Zone II : $1/15 \leq \eta \leq 2/3$

$T = D\tau(\eta);\ \ \tau(\eta) = 2\left[\sqrt{1-\left(\frac{2}{3}-\eta\right)^2} - \frac{2}{3}\right]$

$A = D^2\lambda(\eta)$

$\lambda(\eta) = 1.224814865 - \sin^{-1}\left(\frac{2}{3}-\eta\right) - \left(\frac{2}{3}-\eta\right)\sqrt{1-\left(\frac{2}{3}-\eta\right)^2} - \frac{4}{3}\eta$

$P = D\vartheta(\eta);\ \ \vartheta(\eta) = 1.59610062 - 2\sin^{-1}\left(\frac{2}{3}-\eta\right)$

$R_h = D\frac{\lambda(\eta)}{\vartheta(\eta)}$

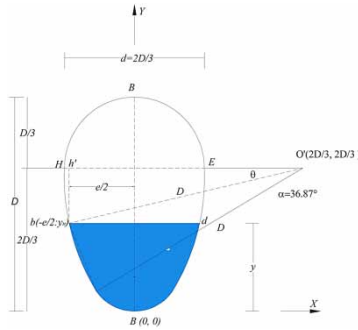

Zone III : $2/3 \leq \eta \leq 1$

$T = D\zeta(\eta);\ \zeta(\eta) = 2\sqrt{(1-\eta)\left(\eta-\frac{1}{3}\right)}$

$A = D^2\delta(\eta)$

$\delta(\eta) = 0.5104589 \ \ + \left(\eta-\frac{2}{3}\right)\sqrt{(1-\eta)\left(\eta-\frac{1}{3}\right)} - \frac{1}{9}\cos^{-1}(3\eta-2)$

$P = D\xi(\eta);\ \xi(\eta) = 2.64329817 - \frac{2}{3}\cos^{-1}(3\eta-2)$

$R_h = D\frac{\delta(\eta)}{\xi(\eta)}$

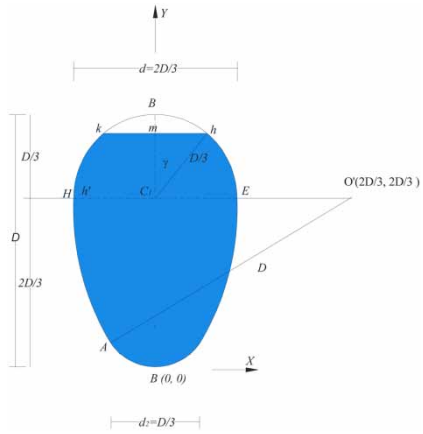

$\eta = y/D$, conduit filling rate; y, flow depth; D, conduit generating diameter; A, wetted area; P, wetted perimeter; T, top width; R_h, hydraulic radius.

is equal to unity and is written very often in the following form (Shang *et al.* 2019):

$$\alpha\frac{Q^2T_c}{gA_c^3} = 1 \tag{1}$$

where α represents the velocity distribution coefficient (generally = 1), Q is the flow rate, g is the acceleration due to gravity, A_c is the critical wetted area and T_c the critical top width.

Furthermore, in a uniform flow occurring in any channel profile, the flow rate can be computed using Achour and Bedjaoui general relationship (2006). This relationship gives the discharge Q as a function of the longitudinal slope S_0, the absolute roughness ε, the wetted area A, the hydraulic radius R_h, and the Reynolds number R^* corresponding to the shear Reynolds number. The relationship is as follows:

$$Q = -4\sqrt{2g}A_n\sqrt{R_{h,n}S_0}\log\left(\frac{\varepsilon}{14.8R_{h,n}} + \frac{10.04}{R^*}\right) \tag{2}$$

With:

$$R^* = 32\sqrt{2}\frac{\sqrt{gR_{h,n}^3S_0}}{\nu} \tag{3}$$

The subscript 'n' denotes normal characteristics of the uniform flow.

3.2. Theoretical development

3.2.1. Normal depth/critical depth relationship

Uniform flow can be found in a subcritical, supercritical or critical regime depending on the importance of its inertia. This importance is reflected either by the value of the Froude number or by opposition of both normal and critical depths. To highlight the type of flow, the calculation of normal and critical depths must be done for the same flow rate.

Eliminating the discharge Q between Equations (1) and (2) and considering that $R_{h,n} = A_n/P_n$, it results:

$$\frac{A_c^{3/2}}{\sqrt{T_c}} = -4\sqrt{2}\frac{A_n^{3/2}}{P_n^{1/2}}\sqrt{S_0}\log\left(\frac{\varepsilon}{14,\,8R_{h,n}} + \frac{10,\,04}{R^*}\right) \tag{4}$$

where the hydraulic radius $R_{h,n}$ is expressed as a function of the generator diameter D and the filling rate η_n (Table 1) and the Reynolds number R^* in Equation (4) is given by the relation (3). Taking into account hydraulic radius relations (Table 1), Reynolds number Equation (3) takes the following form:

$$R^* = 32\sqrt{2}\frac{\sqrt{gD^3S_0}}{\nu}[F_{n,2}]^{3/2} \tag{5}$$

where $F_{n,2}$ functions are regrouped in Table 2.

Table 2 | Expression of the F_c, $F_{n,1}$ and $F_{n,2}$ functions for each zone

Zone	Function		
	F_c	$F_{n,1}$	$F_{n,2}$
Zone I: $\eta \le 1/15$	$\frac{[\sigma(\eta_c)]^{3/2}}{[\varphi(\eta_c)]^{1/2}}$	$\frac{[\sigma(\eta_n)]^{3/2}}{[\rho(\eta_n)]^{1/2}}$	$\frac{\sigma(\eta_n)}{\rho(\eta_n)}$
Zone II: $1/15 \le \eta \le 2/3$	$\frac{[\lambda(\eta_c)]^{3/2}}{[\tau(\eta_c)]^{1/2}}$	$\frac{[\lambda(\eta_n)]^{3/2}}{[\vartheta(\eta_n)]^{1/2}}$	$\frac{\lambda(\eta_n)}{\vartheta(\eta_n)}$
Zone III: $2/3 \le \eta \le 1$	$\frac{[\delta(\eta_c)]^{3/2}}{[\zeta(\eta_c)]^{1/2}}$	$\frac{[\delta(\eta_n)]^{3/2}}{[\xi(\eta_n)]^{1/2}}$	$\frac{\delta(\eta_n)}{\xi(\eta_n)}$

For a full section of the egg-shaped conduit, the flow is governed by the functions of the third zone: $\delta(\eta_n = 1) = 0.5104589$ and $\xi(\eta_n = 1) = 2.64329817$. The Reynolds number R_f* characterizing the full flow section (Achour 2014) is written as:

$$R_f^* = 3.84\frac{\sqrt{gD^3S_0}}{\nu} \tag{6}$$

Taking into account Equations (5) and (6), Reynolds R* number can be related to Reynolds number R_f* at full section as:

$$R^* = 11.784R_f^*[F_{n,2}]^{3/2} \tag{7}$$

For the egg-shaped section, the expressions of the wetted perimeter, the wetted area and the hydraulic radius are written according to the filling zones indicated in Table 1. Therefore, as a result the relation (4) becomes:

$$F_c = -4\sqrt{2}F_{n,1}\sqrt{S_0}\log\left(\frac{\varepsilon/D}{14,\,8F_{n,2}} + \frac{0.852}{R_f^*[F_{n,2}]^{3/2}}\right) \tag{8}$$

The functions F_c, $F_{n,1}$ and $F_{n,2}$ are expressed exclusively according to the filling rate of the pipe and are grouped in Table 2.

In the results and discussion section, the in-depth study of Equation (8) will allow describing the nature of the flow and some interesting conclusions will be drawn.

3.2.2. Froude number relationship

In any study that attempts to characterize the nature of the flow regime, the Froude number value is calculated as a function of the flow rate and geometric characteristics of the given section. In order to make the calculation of the Froude number easier, a highly interesting approach will be developed and used as an alternative technique. By using the general form of Froude number relationship:

$$F_r^2 = \frac{Q^2T_n}{gA_n^3} \tag{9}$$

By combining the Equations (2) and (9), one may obtain:

$$F_r = -4\sqrt{2}\left(\frac{T_n}{A_n}\right)^{1/2}\sqrt{R_{h,n}S_0}\log\left(\frac{\varepsilon}{14.8R_{h,n}} + \frac{10.04}{R^*}\right) \tag{10}$$

From Equation (7) and Table 1, Equation (10) becomes:

$$F_r = -4\sqrt{2}F_{n,3}\sqrt{S_0}\log\left[\frac{\varepsilon/D}{14.8F_{n,2}} + \frac{0.852}{R_f^*(F_{n,2})^{3/2}}\right] \tag{11}$$

where the functions of $F_{n,2}$ are given by Table 2, while $F_{n,3}$ functions are expressed as:

$$F_{n,3} = \begin{cases} [\varphi(\eta_n)/\rho(\eta_n)]^{1/2} & Zone\,I \\ [\tau(\eta_n)/\vartheta(\eta_n)]^{1/2} & Zone\,II \\ [\zeta(\eta_n)/\xi(\eta_n)]^{1/2} & Zone\,III \end{cases}$$

In Equation (11), the Froude number is expressed as a function of the slope S_0, the generating diameter D of the conduit, the functions $F_{n,2}$ and $F_{n,3}$ containing the filling rate η, the absolute roughness ε and the Reynolds number R_f* at the full state of the conduit which takes into account the effect of the kinematic viscosity ν. It is worth noting that Equation (11) takes into account all the flow parameters that allow a better representation of the natural phenomenon. It is necessary also to specify

that Equation (11) allows the explicit calculation of the Froude number independently of the volume flow rate. Moreover, in the absence of the flow rate value, Equation (11) provides a basis for determining the nature of the flow regime. However, it is necessary to analyze this relationship graphically in order to examine the flow behavior according to the importance of the slope value. To highlight the developed expressions, graphs will be constructed in a Cartesian coordinate system considering a smooth egg-shaped conduit of generating diameter D equal to unity.

4. RESULTS AND DISCUSSION

4.1. Analysis of the normal depth/critical depth relationship

For a better visibility of Equation (8), it is essential to use a graphic representation expressing the influence of the slope in the production of the different types of flows and consequently the number of critical states that can possibly occur in the conduit. For this purpose, as an example, a smooth egg-shaped conduit ($\varepsilon \to 0$) with a diameter $D = 1$ m is considered. Figure 1 shows the variation of the filling rate η_c at the critical state as a function the relative normal depth η_n for longitudinal slope S_0 range usually encountered in the practice of the hydraulic engineer.

In Figure 1, the first bisector represents the critical state of the flow corresponding to $\eta_c = \eta_n$. This limit makes it possible to differentiate two domains of flow regimes, namely: the subcritical and supercritical domains. Moreover, one may note that some curves remain below this line. Therefore, no critical condition can be observed in this area and the predominant regime is subcritical.

This can be explained by the fact that for low slopes, the gravity forces prevail over inertia forces regardless the variation in the filling rate. Therefore the developed energy does not allow a transition to the supercritical regime; the limit of this zone is marked by the curve tangent to the first bisector characterized by a slope $S_0 = 0.00241096$ (Figure 2).

By examining the curve $\eta_c = f(\eta_n)$ in Figure 2, it is clear that only one critical condition can occur. This state is observed at the point tangent to the first bisector which corresponds to $\eta_c = \eta_n \approx 0.2$. In addition, it should be noted that the limit curve which gives a single critical state presents a maximum for $\eta_{c,max} \approx 0.762$ corresponding to $\eta_n(\eta_{c,max}) \approx 0.955$.

Beyond this limit curve, the curves intersect the first bisector at two points, thus indicating the existence of two critical states at two different flow rates.

Figure 3 illustrates an example of the two critical states generated for the slope $S_0 = 0.003$.

Regarding Figure 3, one can observe that the curve $\eta_c = f(\eta_n)$ corresponding to the slope $S_0 = 0.003$ intercepts the curve of the critical flow regime (Red line) at two points thus indicating the presence of two critical regimes for this slope.

Figure 3(a) represents the first point of intersection with a low filling rate $\eta_c = \eta_n = 0.0311162 \approx 0.031$ while the second point of intersection is obtained at a higher filling rate $\eta_c = \eta_n = 0.618078 \approx 0.618$ as shown in Figure 3(b).

4.2. Froude number relation study

In the previous section, a method has been developed from which it is possible to deduce the different states of the flow in the pipe by the combination of both normal and critical flows. At the same time, it is interesting to note that it is easy to

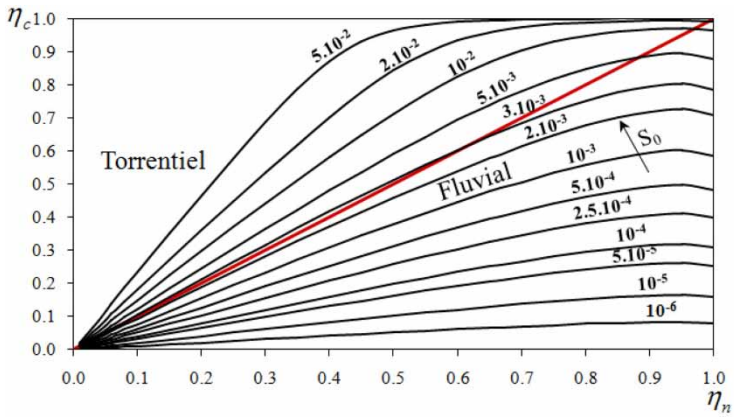

Figure 1 | Variation of η_c depending on η_n for slopes values S_0 according to Equation (8) for smooth conduit.

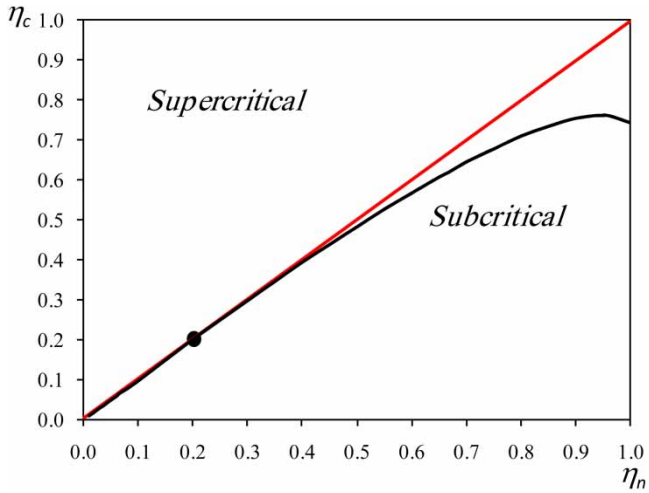

Figure 2 | Curve of variation of η_c according to η_n tangent to the first bisector. Slope: $S_0 = 0.00241096$, (•) $\eta_n = \eta_c = 0.199997835 \approx 0.2$, $\eta_{c,max} \approx 0.762$, $\eta_n(\eta_{c,max}) \approx 0.955$.

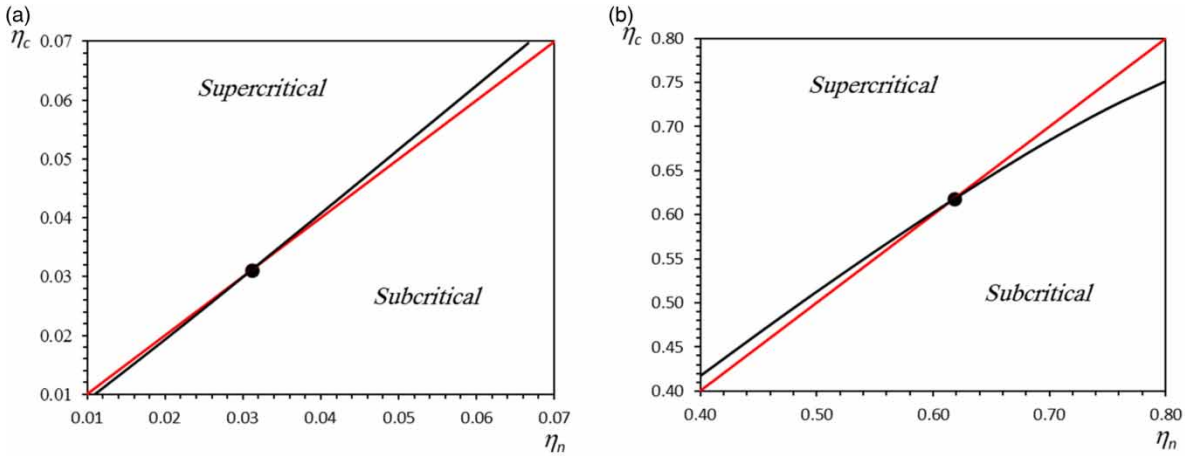

Figure 3 | Variation between η_c and η_n for the slope $S_0 = 0.003$.

characterize flows by an elementary analysis of normal flow exclusively. For this purpose, the variation of the Froude number as a function of the filling rate η for different slopes S_0 was represented graphically in Figure 4 according to Equation (11).

In Figure 4, the horizontal bold line (in red color) corresponds to Froude number $F_r = 1$. It should be noted that below this line the flow regime is subcritical, i.e. $F_r < 1$, while the flow regime is supercritical in the zone above the line, i.e. $F_r > 1$. For slope values greater than the limit slope, it is noted that, for a given slope and for two different flow rates, the critical regime appears initially for low filling rates then at higher filling rates. On the contrary, for certain values of the slope S_0, the curves are entirely in the zone of the subcritical regime thus indicating that no critical regime can occur. In addition, a limit curve characterized by a point of tangency with the horizontal red line indicates the existence of a single critical condition corresponding to the limit slope $S_0 = 0.00241096$ and the filling rate $\eta \approx 0.2$ (Figure 5).

5. VALIDATION

The minimum specific energy leads to a critical regime and consequently it can be used as a method of validating the results obtained in the previous section. The basic equation for specific energy is written:

$$E_s = y_n + \frac{Q^2}{2gA^2} \tag{12}$$

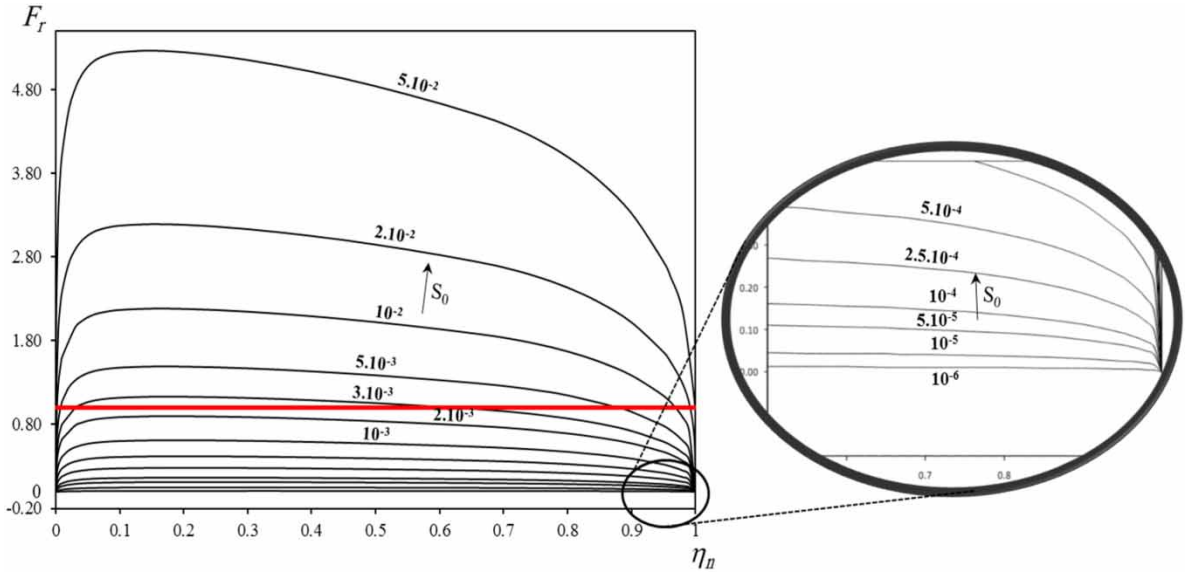

Figure 4 | Variation curves of Froude number F_r as a function of the filling rate η_n according to Equation (11) for smooth conduit.

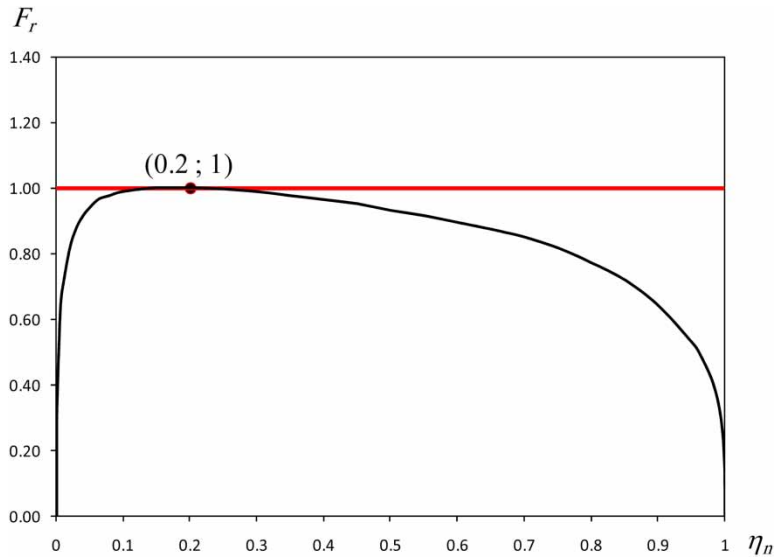

Figure 5 | Point of tangency. Slope: $S_0 = 0.00241096$, E/D=0, (•) $\eta_n = \eta_c = 0.199997835 \approx 0.2$.

In Equation (12), the wetted area A is given by Table 1. By dividing the specific energy of relation (12) by the generating diameter D, one may obtain the dimensionless specific energy: $E_s^* = E_s/D$. Equation (12) is then reduced to:

$$E_s^* = \eta_n + \frac{Q^{*2}}{F_{n,4}} \tag{13}$$

With: $\eta_n = y_n/D$, $Q^* = Q/\sqrt{gD^5}$ and the function $F_{n,4}$ is written according to the filling rate as follows:

$$F_{n,4} = \begin{cases} 2[\sigma(\eta_n)]^2 & Zone\,I \\ 2[\lambda(\eta_n)]^2 & Zone\,II \\ 2[\delta(\eta_n)]^2 & Zone\,III \end{cases}$$

Considering the filling rate η_n, the relative flow rate Q^* is expressed according to relations (2), (7) and Table 1, as:

$$Q^* = -4\sqrt{2}F_{n,1}\sqrt{S_0}\log\left(\frac{\varepsilon/D}{14.8F_{n,2}} + \frac{0.852}{R_f^*(F_{n,2})^{3/2}}\right) \tag{14}$$

Note that the functions $F_{n,1}$ and $F_{n,2}$ are detailed in Table 2.

The results obtained in the previous section can be validated using relations (13) and (14).

Figure 6 shows the curve form of the relative specific energy $E_S{}^*$ variability based on the filling rate η_n. For all the slopes above, the first bisector (Figure 1), or at the right side of $F_r = 1$ (Figure 4), where the curves have two critical states, the slope $S_0 = 0.003$ was taken as an example of validation process.

In Figure 6, it appears that the minimum relative specific energy perfectly coincides with the two critical states observed for the slope ($S_0 = 0.003$; E/D = 0) taken as an example.

6. FLOW STATES

In order to characterize the boundaries between the different states of uniform flow in an egg-shaped pipe, it would be judicious to plot the curves characterized by the critical states according to the Equation (8) by substituting the « n » index expressing normal flow with that of the critical flow « c ». Therefore, the relation expressing the slope S0 is written:

$$S_0 = \frac{1}{32}\left[F_{c,3}\log\left(\frac{\varepsilon/D}{14.8F_{c,2}} + \frac{0.852}{R_f^*(F_{c,2})^{3/2}}\right)\right]^{-2} \tag{15}$$

Note: functions $F_{c,2}$ and $F_{c,3}$ correspond in this case to $F_{n,2}$ and $F_{n,3}$ respectively.

Figure 7 shows the variation of the slope S_0 as a function of the critical depth according to relation (15) for a smooth egg-shaped conduit. The dashed line curve expresses the variation of the slope S_0 as a function of the maximum Froude number.

Through Figure 7 it is possible to deduce:

1. Zone I: The depths are weak and the regime is subcritical.
2. Zone II: The regime is supercritical and the boundary between zones I and II is marked by passing through a critical regime.
3. Zone III: At strong depths, the regime is again subcritical and the transition is made through a second passage by the critical regime.
4. Zone IV: Mild slope zone where no critical regime can occur. The flow is uniform and subcritical, bordered by the maximum values of Froude number.

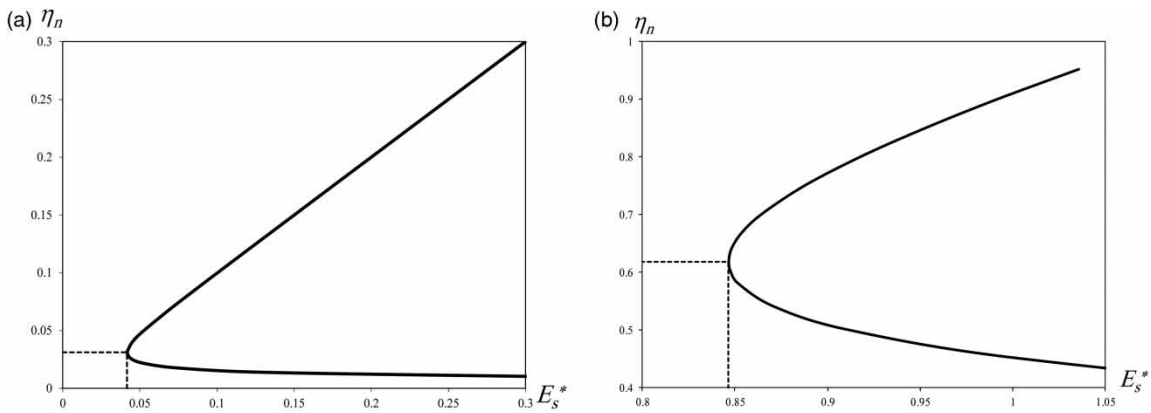

Figure 6 | Variation curve for relative specific energy based on filling ratio ($S_0 = 0.003$; E/D = 0). (a) $\eta_n = \eta_c = 0.0311162$, $E_S{}^*{}_{min} = 0.04169881$, $Q^* = 0.000597196$. (b) $\eta_n = \eta_c = 0.618078$, $E_S{}^*{}_{min} = 0.846566461$, $Q^* = 0.205214732$.

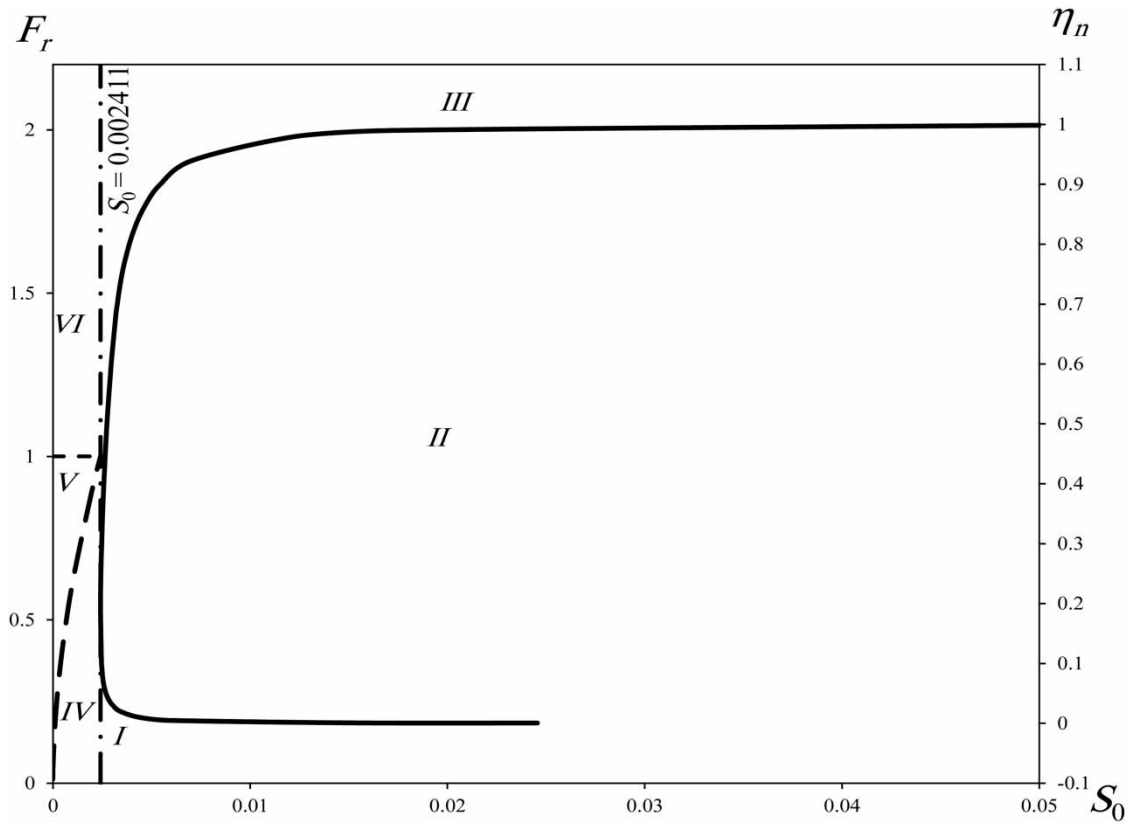

Figure 7 | Different flow states in smooth egg shaped conduit. (——) The slope changes with the fill rate. (— —) Slope variation according to Froude number. (— · —) Straight line corresponding to $S_0 = 0.002411$.

5. Zone V: In this area, the uniform flow is improbable, the values of the Froude number are less than unity; the slopes are weak so the flow is, eventually, gradually varied type (backwater).
6. Zone VI: In this zone, the uniform flow is also implausible, the values of the Froude number are greater than unity, and the slopes are weak, therefore the flow is suddenly varied (hydraulic jump). The demarcation between zones V and IV denotes the passage by a fictitious critical regime.

7. CONCLUSION

It was possible during this work to achieve a functional relationship between critical depth and normal depth for egg-shaped conduit. This relation has been represented graphically for slopes varying between 10^{-6} and 5.10^{-2}. The analysis of the obtained curves shows the existence of different states of critical flow in the conduit. Indeed, it has been observed that for the limit slope $S_0 = 0.00241096$; E/D = 0 a single critical regime is possible, also for slopes less than this slope, no critical regime can occur and for higher slopes two critical states are possible.

However, a highly interesting relation has been developed in order to calculate the Froude number independently of the flow rate. The graphic representation of this relationship confirmed the observations mentioned above. Still, the curve of variation of the normal depth according to the strong slope on the one hand, and the Froude number according to the mild slopes on the other hand, lead to the establishment of six zones regrouping the different types of flows encountered in the practice. Validation of the obtained results was possible through the analysis of the specific energy for a slope $S_0 = 0.003$.

Finally, it is important to note the need for further study in order to examine the effect of the generating diameter and absolute roughness on critical flow.

DATA AVAILABILITY STATEMENT

All relevant data are included in the paper or its Supplementary Information.

REFERENCES

Achour, B. 2014 *Ecoulement Uniforme Dans la Conduite de Forme Ovoïdale*. Editions universitaires europeennes. OmniScriptum GmbH & Co. K.G. Publishing Group, Saarbrucken, Germany.

Achour, B. & Amara, L. 2020 New theoretical considerations on the critical flow in a circular conduit (part 1). *Larhyss Journal* **17** (43), 103–118.

Achour, B. & Bedjaoui, A. 2006 Exact solutions for normal depth problem. *Journal of Hydraulic Research* **44** (5), 715–717.

Butler, D. & Davies, J. W. 2010 *Urban Drainage*. Spon Press, London, UK and New York, NY, USA.

Chow, V. T. 1959 *Open-channel Hydraulics*. McGraw-Hill, Tokyo, Japan.

French, R. H. 1985 *Open-channel Hydraulics*. McGraw-Hill, New York, NY, USA.

Heggen, R. 1991 Critical depth, velocity profile, and channel shape. *Journal of Irrigation and Drainage Engineering* **117** (3), 442–448.

Henderson, F. M. 1966 *Open Channel Flow* MacMillan Company, New York, NY, USA.

Lakehal, M. & Achour, B. 2014 Calcul de la profondeur normale dans une conduite ovoïdale par la methode du modele rugueux (Computation of normal depth in an egg-shaped conduit using the rough model method). *Larhyss Journal* **11** (3), 101–103.

Nebbar, M. L. & Achour, B. 2018 Design of rectangular channel at critical flow. *Larhyss Journal* **15** (2), 7–20.

Petikas, I., Keramaris, E. & Kanakoudis, V. 2020 Calculation of multiple critical depths in open channels using an adaptive cubic polynomials algorithm. *Water* **12** (3), 799.

Regueiro-Picallo, M., Naves, J., Anta, J., Puertas, J. & Suárez, J. 2016 Experimental and numerical analysis of egg-shaped sewer pipes flow performance. *Water* **8** (12), 587.

Shang, H., Xu, S., Zhang, K. & Zhao, L. 2019 Explicit solution for critical depth in closed conduits flowing partly full. *Water* **11** (10), 2124.

Straub, W. O. 1982 Personal communication, Civil Engineering Associate. Department of Water and Power, City of Los Angeles, CA, USA.

Suarez, J. & Puertas, J. 2005 Determination of COD, BOD, and suspended solids loads during combined sewer overflow (CSO) events in some combined catchments in Spain. *Ecological Engineering* **24** (3), 199–217.

Swamee, P. K. 1993 Critical depth equations for irrigation canals. *Journal of Irrigation and Drainage Engineering* **119** (2), 400–409.

Swamee, P. K. & Rathie, P. N. 2005 Exact equations for critical depth in a trapezoidal canal. *Journal of Irrigation and Drainage Engineering* **131** (5), 474–476.

Swamee, P. K. & Swamee, N. 2008 Design of noncircular sewer sections. *Journal of Hydraulic Research* **46** (2), 277–281.

Vatankhah, A. R. & Easa, S. M. 2011 Explicit solutions for critical and normal depths in channels with different shapes. *Flow Measurement and Instrumentation* **22** (1), 43–49.

Vatankhah, A. R. 2015 Critical and normal depths in semielliptical channels. *Journal of Irrigation and Drainage Engineering* **141** (10), 06015002.

Wang, Z. 1998 Formula for calculating critical depth of trapezoidal open channel. *Journal of Hydraulic Engineering* **124** (1), 90–91.

First received 11 May 2021; accepted in revised form 25 June 2021. Available online 12 July 2021